Journal of Nuclear and Particle Physics 2015, 5(6): 101-111
DOI: 10.5923/j.jnpp.20150506.02

Mossbauer Spectroscopy, Electrical Transport Properties and Gamma-Ray Attenuation Coefficients of Some Sodium-Iron-Phosphate Glasses Containing Bismuth

A. M. Abdel-Ghany[1], T. Z. Amer[2], A. A. Bendary[3], A. G. Mostafa[3,*]

[1]Basic Science Dept., Faculty of Engineering Science, Sinai Univ., El-Arish, Egypt
[2]Phys. Dept., Faculty of Science, Al-Azhar Univ., (Girls Branch), Nasr City, Cairo, Egypt
[3]Mossbauer Lab., Phys. Dept., Faculty of Science, Al-Azhar Univ., Nasr City, Cairo, Egypt

Abstract Some sodium iron phosphate glasses containing different amounts of bismuth have been prepared by the melt quenching method. The hyperfine structure of iron was characterized by Mossbauer effect (ME) spectroscopy. The density and molar volume were measured experimentally and were calculated empirically for comparison. Mossbauer spectroscopy showed the presence of two oxidation states of iron (Fe^{2+} and Fe^{3+}) where all Fe^{2+} ions occupied the tetrahedral coordination, while Fe^{3+} ions appeared in both the tetrahedral and octahedral coordination states. The dc conductivity temperature dependence appeared to follow an Arrhenius type behavior while the frequency dependence ac conductivity follows a simple power law feature. The CBH model was found to be the most applicable conduction mechanism. It was found that, as Bi_2O_3 was gradually increased the gamma-ray mass attenuation coefficient increased while the HVL decreased, and the sample containing 10 mol% Bi_2O_3 can be used as good shielding material for low gamma-ray photon energies.

Keywords Iron-bismuth-phosphate glasses, Mossbauer spectroscopy, Semi-conducting glasses, Electrical transport properties, Density & molar volume, Gamma-ray mass attenuation coefficient and Shielding glasses

1. Introduction

Iron-sodium-phosphate glasses exhibit both electronic and ionic conductivities and have been studied extensively because of their low melting point and strong glass-forming character. Such glasses represent potential candidates for energy storage devices and solid state batteries as well as many applications in medical use [1-5].

It is known that Bi_2O_3 cannot form glass like other traditional glass formers, but it can form glass in the presence of any conventional glass former [6]. In such glasses, high polarizing Bi(III) ion can reduce its coordination number from six to three and thus glass network may consist of both BiO_6 highly distorted octahedral and BiO_3 pyramidal units [7]. It is known also that, the addition of iron and / or bismuth cations increases the aqueous durability of phosphate glasses through the formation of P–O–Fe and / or P–O–Bi bonds [8, 9]. The formation of such bonds affects directly different properties of phosphate glasses [10, 11]. Shaim and Et-Tabirou [12] have investigated the electrical transport properties of some alkali phosphate glasses containing Bi_2O_3. They concluded that, the electrical conductivity of such glasses depends on their composition and preparation technique [13, 14]. It is found that, when a network former oxide is substituted for another one, the conductivity of such mixed-former glasses exhibits different behaviors [15]. Most of the disordered materials show a dielectric relaxation that does not described by an exponential (Debye-like) decay with a characteristic single decay time [16].

On the other hand, iron-phosphate glasses containing Bi_2O_3 have drawn much attention due to their high gamma-ray attenuation coefficient, which reflects the possibility to act as good shielding material as well as for nuclear waste encapsulation [17]. However, Saudi et al have studied the gamma-ray attenuation coefficient and half value layer (HVL) of some glasses containing Bi_2O_3 and CdO, where they found that the formation of some P-O-Bi bonds cause a relative increase in the density of these glasses as well as their mass attenuation coefficient [18]. Mostafa et al, have studied the gamma-ray attenuation coefficient of some silicate glasses containing Bi_2O_3, where the used silica was extracted from rice husk ash. They found that the glass sample containing 20 mol% Bi_2O_3 is suitable for attenuating low gamma-ray photon energies while that contains 5 mol% Bi_2O_3 exhibits the highest neutron removal cross- section [19].

* Corresponding author:
drahmedgamal@yahoo.com (A. G. Mostafa)
Published online at http://journal.sapub.org/jnpp

However, in this article, the hyperfine structure of some iron-sodium-phosphate glasses containing different amounts of bismuth oxide will be thoroughly investigated, applying Mossbauer spectroscopy. Then, the electrical transport properties as well as the gamma-ray mass attenuation coefficients and the HVL, will be also studied.

2. Experimental

Iron-sodium-phosphate glasses doped with bismuth having the composition,

20 mol% Fe_3O_4. 20 mol% Na_2O. (60-x) mol% P_2O_5. (x) mol% Bi_2O_3,

[where $0 \leq x \leq 10$ in steps of 2.5]

have been prepared using pure Fe_3O_4, B_2O_3, Na_2CO_3 and (NH_4) H_2PO_4 as starting materials. The batches were mixed well and melted in porcelain crucibles in an electrically heated muffle furnace at 1100°C for 2 h with frequent stirring to ensure complete homogeneity. Melts were then rapidly quenched onto a pre-cooled stainless steel molds in air.

Mossbauer spectra were obtained using a constant acceleration Mössbauer effect spectrometer and the Mossbauer parameters were calculated relative to metallic iron calibration spectrum.

For electrical conductivity measurements, the obtained solid glasses were polished to obtain disk shape samples of 1 mm thickness and 7 mm diameter with optically flat surfaces coated with silver paste. Each sample was then placed in a cell between two copper disks and the temperature of the sample was measured using a chromel–alumel thermocouple. All measurements were carried out in the temperature range from 300 to 525 K at four fixed frequencies [0.12, 1, 10 and 100 kHz], using RLC bridge (model SR–270).

Density measurements were carried out by the liquid displacement method in toluene as an emersion liquid at room temperature using an electric balance of 10^{-4} g sensitivity. The molar volume values were then calculated from the obtained density results.

The gamma-ray mass attenuation coefficients of the studied glasses have been calculated using WIN-X-COM program based on the mixture rule, and the HVL values were then calculated from the obtained results.

3. Results and Discussion

3.1. Mossbauer Spectroscopic Analysis

All the obtained Mossbauer spectra appeared to be generally similar, and Figure (1) represents the obtained Mossbauer spectra of the glass samples containing 0 and 10 mol% Bi_2O_3. The computer analysis and fitting indicated that three separated paramagnetic doublets are presented in each spectrum, and the calculated parameters are exhibited in Table (1). Inspecting these parameters, it can be seen that the line width (LW) values of phase (I) appeared to fluctuate between 0.57 and 0.38 mm/s, while that of phase (II) appeared to fluctuate between 0.44 and 0.35 mm/s and that of phase (III) appeared to fluctuate between 0.39 and 0.51 mm/s. That is, all LW values appeared to be highly broadened which reflect the amorphous and glassy state nature of the studied samples.

It is observed that the isomer shift (IS) values of phase (I) are found in between 1.12 and 0.98 mm/s while that of phase (II) appeared in between 0.52 and 0.44 mm/s and that of phase (III) appeared to fluctuate between 0.43 and 0.36 mm/s. On the other hand, the Quadrapole splitting (QS) values of phase (I) fluctuated between 2.49 and 2.43 mm/s but that of phase (II) was found between 0.98 and 0.78 mm/s, while that of phase (III) appeared to fluctuate between 0.66 and 0.54 mm/s.

It is observed also, from the calculations of the area under the Mossbauer absorption peeks of each phase, that as Bi_2O_3 was gradually increased at the expense of P_2O_5, Fe^{2+} increased from 10.7% to 28.1% while Fe^{3+} decreased from 89.3% to 71.9%. On the other hand and by calculating the total Fe(T) and Fe(O), it appeared that the tetrahedral symmetry increased from 56.8% to 85.7%, while the octahedral symmetry decreased from 43.2% to 14.3%. This can be taken as evidence that, the introduced Bi cations occupy the glass network modifier (GNM) positions, and hence force some iron cations to occupy the glass network former (GNF) positions.

Table (1). The obtained Mossbauer parameters for all iron phases in the studied glasses

Sample	IS(mm/s)	QS(mm/s)	LW(mm/s)	A%	Assignment
1	0.98	2.48	0.38	10.7	Fe^{2+}(T)
	0.52	0.78	0.44	46.1	Fe^{3+}(T)
	0.35	0.66	0.41	43.2	Fe^{3+}(O)
2	1.08	2.42	0.49	23.6	Fe^{2+}(T)
	0.44	0.94	0.35	33.5	Fe^{3+}(T)
	0.41	0.57	0.39	42.9	Fe^{3+}(O)
3	1.11	2.46	0.57	26.5	Fe^{2+}(T)
	0.44	0.98	0.35	25.2	Fe^{3+}(T)
	0.43	0.58	0.43	48.3	Fe^{3+}(O)
4	1.12	2.47	0.52	26.5	Fe^{2+}(T)
	0.44	0.88	0.44	43.8	Fe^{3+}(T)
	0.4	0.55	0.39	29.7	Fe^{3+}(O)
5	1.09	2.49	0.5	28.1	Fe^{2+}(T)
	0.44	0.85	0.44	57.6	Fe^{3+}(T)
	0.41	0.54	0.47	14.3	Fe^{3+}(O)

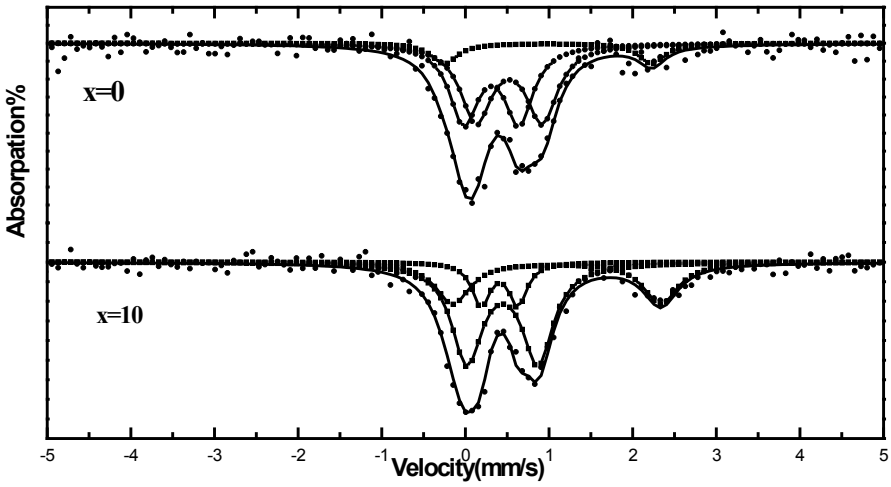

Figure (1). The obtained Mossbauer spectra of the samples containing 0 and 10 mol% Bi_2O_3, as representative spectra

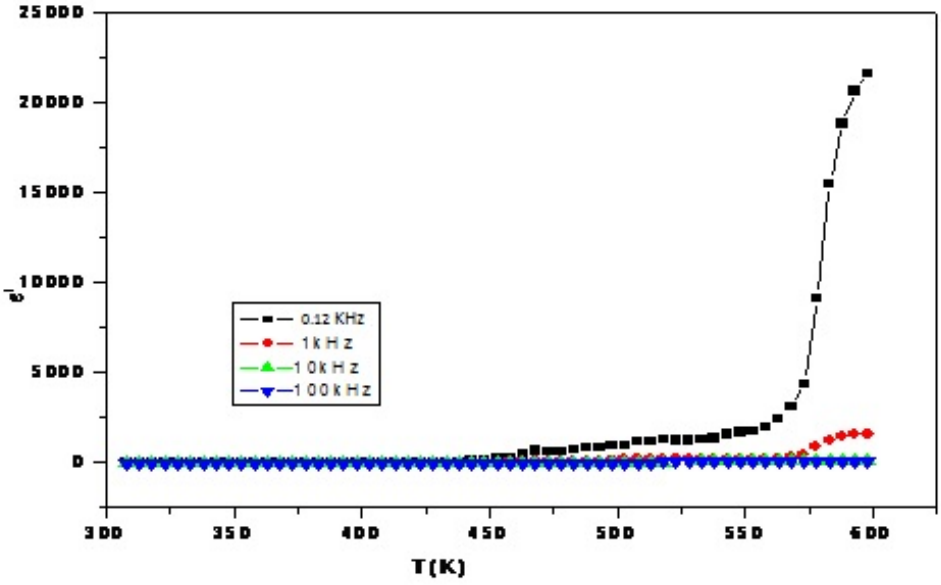

Figure (2). The dielectric constant (ε') temperature dependence at four different frequencies for the sample containing 7.5 mol% Bi_2O_3, as representative curve

According to the obtained parameters, it can be stated that iron ions occupy two different oxidation states (Fe^{2+} and Fe^{3+}) and all Fe^{2+} occupy tetrahedral coordination symmetry indicating that all Fe^{2+} act as GNF. On the other hand, Fe^{3+} ions was found to occupy two different phases, one with tetrahedral symmetry indicating that iron cations in this phase act also as GNF, while the iron cations in the second phase appeared in the octahedral symmetry indicating that they occupy the interstitial positions acting as GNM [20, 21].

However, it is worth to conclude that, all the studied samples are of pure glassy state and pure paramagnetic character. Slight fluctuation in the QS and IS values are observed indicating very slight variations in the electric field gradient (EFG) as well as slight structural changes affect the wave function of the s-electron density at the nucleus of the iron ions. This may be due to the randomness character of the glass networks, as well as the gradual transformation of some Fe^{3+} to Fe^{2+} cations and the increase of some Fe(T) at the expense of Fe(O) coordination symetry in the glass matrices [22, 23].

3.2. Electrical Transport Properties

In this section the dielectric properties as well as the dc and ac electrical conductivities of the studied glasses were

thoroughly investigated.

3.2.1. Dielectric Properties

The temperature dependence of the dielectric constant (ε′) of the sample containing 7.5 mol% Bi_2O_3 can be shown in Figure (2), at four different frequencies (0.12, 1, 10 and 100 kHz) and generally, all samples show similar behavior. From this figure, it can be noticed that at low temperature (below 430 K) the dielectric constant appeared to be temperature independent, while at high temperature (above 430 K), it increases gradually as the temperature was increased such that the rate of increase is inversely proportional to the frequency. This behavior can be attributed to the fact that the orientational polarization is related to the thermal motion (vibration) of the molecules [24] and/or to the space charge polarization due to the bonding defects in the network structure [25].

3.2.2. Pseudo Cole-Cole Diagram

Pseudo Cole-Cole diagram had been suggested, instead of the conventional Cole–Cole plot between ε″ (ω) and ε′ (ω), at fixed temperature [26], such that ε″ (T) and ε′ (T) can be plotted at a fixed frequency. In the present work, pseudo Cole-Cole diagram was obtained by plotting the imaginary part of the electric modulus (M″ (T)) against its real part (M′ (T)) at constant frequency, where M_1 and M_2 are calculated from equations (1) and (2) respectively.

$$M' = \varepsilon' / (\varepsilon'^2 + \varepsilon''^2) \quad (1)$$

$$M'' = \varepsilon'' / (\varepsilon'^2 + \varepsilon''^2) \quad (2)$$

Figurer (3) shows the obtained pseudo Cole-Cole diagram at 100 kHz for the sample containing 7.5 mol% Bi_2O_3. It is clear that all plots of M″ (T) ~ M′(T) show a single semicircle, indicating a single relaxation process which agree well with that predict from Cole- Cole diagram.

Figurer (4) exhibits the imaginary part of the electric modulus M″ (T) as a function of temperature, at four different frequencies (0.12, 1, 10 and 100 kHz). It is observed generally that for all the studied samples M″ shows a single relaxation peak at a certain temperature T_m. This peak shifted to a higher temperature as the frequency was increased, showing the relaxation character of the dielectric loss of such sample [26]. This behavior (relaxation phenomena) can be attributed to frequency dependence of the orientational polarization (dipolar dielectrics) [27].

3.2.3. D.C. Conductivity Calculation

The dc conductivity has been obtained from the extrapolation of the frequency independent plateau region of the (ln σ_t verses ln ω) plot according to equation (3),

$$\sigma_{total} = A\,\omega^s + \sigma_{dc} \quad (3)$$

where (σ_{dc}) is the frequency independent dc conductivity, (A) is a weakly temperature dependent quantity and (s) is the exponent factor which lies in the range $0 \le s \le 1$.

As a representative curve, Figure (5) shows the frequency dependent conductivity (ln σ verses ln ω) of the sample containing 7.5 mol% Bi_2O_3, at a definite temperature (473 K). The conductivity was found to be almost frequency independent at low frequency region, and a similar behavior was observed for all the studied samples.

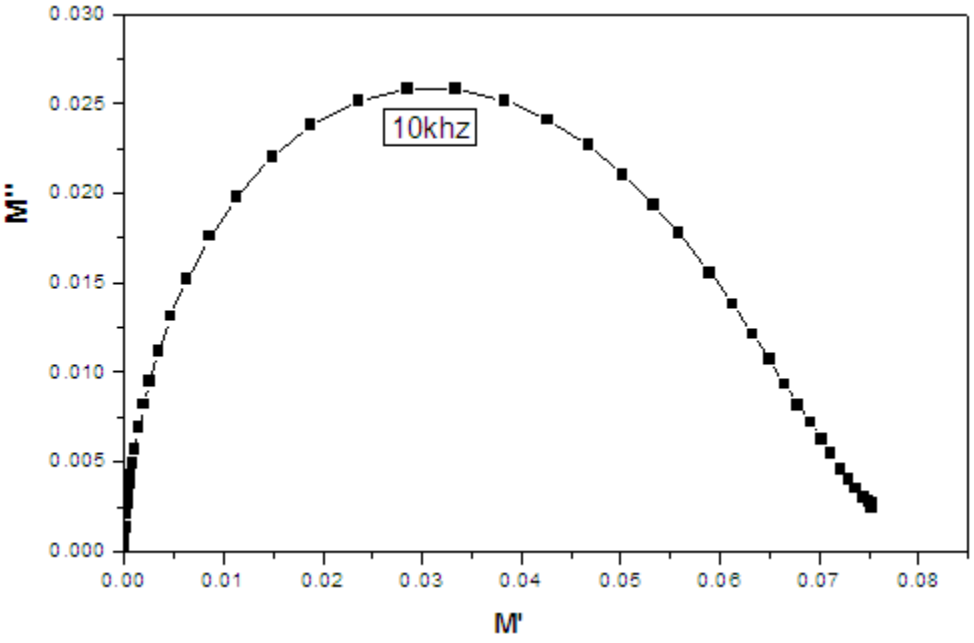

Figure (3). Pseudo Cole-Cole diagram at 100 KHz for the sample containing 7.5 mol% Bi_2O_3, as representative curve

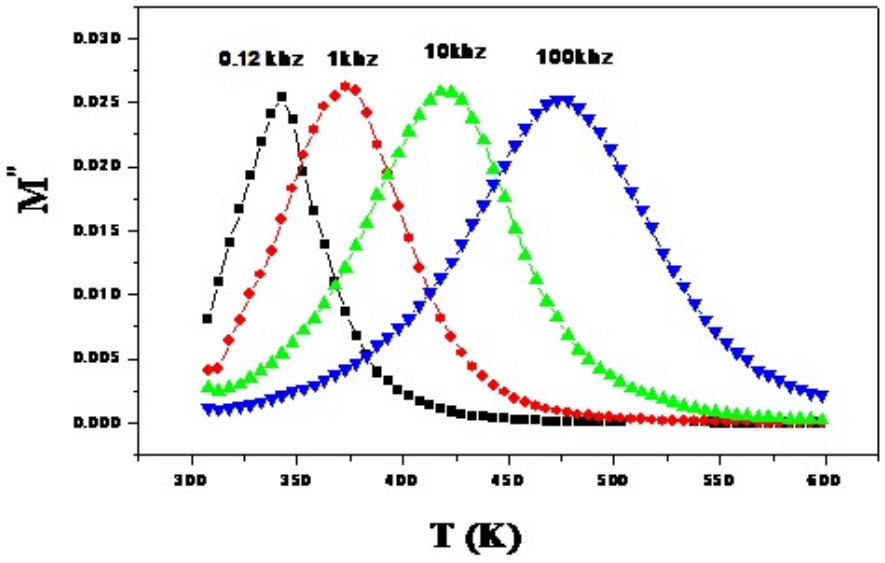

Figure (4). The variation of M″ with temperature at four different frequencies for the sample containing 7.5 mol% Bi_2O_3, as representative curve

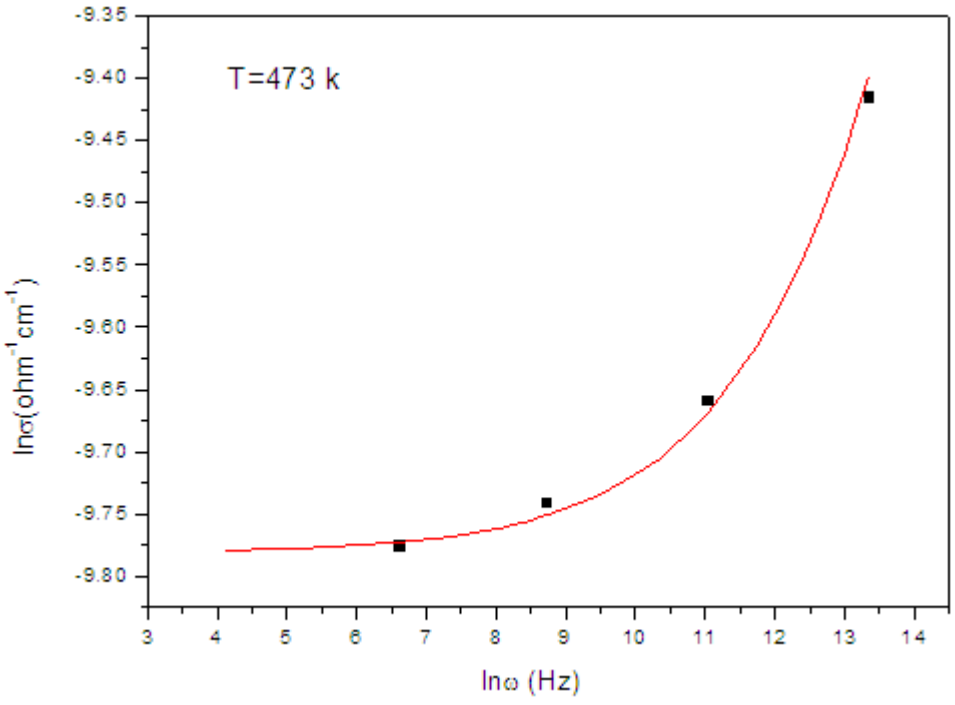

Figure (5). The frequency dependent conductivity of the sample containing 7.5 mol% Bi_2O_3, as representative curve

The obtained dc conductivity values were plotted as a function of (Bi_2O_3) at T = (473°K) in Figure (6). It is appeared that as Bi_2O_3 was increased gradually, the dc conductivity increased approximately linearly. This increased may be due to both:

1. The gradual increase of the large Bi^{3+} cations which act to open gradually the glass network, and hence to ease the mobility of the present Na^+ cations.
2. The gradual increase of Fe^{2+} cations at the expense of Fe^{3+} which act to increase the electron hopping between both cations.

3.2.4. A.C. Conductivity

The ac conductivity of all amorphous materials and glasses follows the universal power law of the form (equation (4)),

$$\sigma_{ac} = A\,\omega^s \quad (4)$$

The obtained temperature dependence of the exponent factor (s) for all the investigated glasses show approximately similar behavior, and Figure (7) shows the change of the s-factor as a function of temperature for the sample containing 7.5 mol% Bi_2O_3, as representative curve. The values of s was found to decrease as the temperature was

gradually increased. Different models were applied in order to conclude the possible conduction mechanism. An agreement was found between the obtained experimental data and those predicted by the correlated barrier-hopping (CBH) model. In this model, the s- factor is temperature dependent as shown from equation (5),

$$s = 1 - \frac{6k_B T}{W_m + k_B T \ln(\omega \tau_\circ)} \quad (5)$$

where τ_o, W_m, T, ω and k_B are the static relaxation time, ac activation energy, absolute temperature, angular frequency and Boltzmann constant respectively. So it can be supposed that the CBH is the applicable model that can be used to describe the conduction mechanism of the investigated glasses [27].

The experimentally obtained temperature dependence of the ac conductivity of the sample containing 7.5 mol% Bi_2O_3 can be seen in Figure (8) as a representative curve. It is appeared that at high temperature the ac conductivity shows strong temperature dependence and weak frequency dependence, while at low temperature the ac conductivity shows weak temperature dependence and strong frequency dispersion. It is appeared also that the ac conductivity values increased with the increase of frequency which may be due to the strong dispersion of both the real and the imaginary parts of the dielectric properties [28]. A similar behavior was observed for all the studied glasses.

However, inspecting all the obtained results in this section, it can be supposed that all glasses behave like semiconductors and both ionic and electronic conductivity are present. The conductivity shows gradual increase with the increase of Bi^{3+} cations. This increase may supposed to be due to the increase of the mobility of Na^+ cations and the increase of the electron hopping between Fe^{2+} and Fe^{3+} cations. It can be supposed also that the predominant conduction mechanism is the CBH model. Also the obtained electrical parameters were found to depend on the glass composition and the measuring conditions (temperature and frequency).

3.3. Density and Molar Volume

The experimental density values ($\boldsymbol{\rho_{exp}}$) were measured applying Archimedes method, using toluene as an emersion liquid, applying equation (6),

$$\rho_{\exp} = \frac{M_a}{M_a - M_t}\ \rho_t \quad (6)$$

where $\boldsymbol{\rho_t}$ is the density of toluene, $\boldsymbol{M_a}$ and $\boldsymbol{M_t}$ is the mass of a sample in air and in toluene respectively. Then the empirical density values ($\boldsymbol{\rho_{emp}}$) of the corresponding close packed structural compounds were also calculated applying equation (7),

$$\rho_{emp} = \sum X_i \rho_i \quad (7)$$

where $\boldsymbol{\rho_i}$ are the densities of the oxides forming a glass, and $\boldsymbol{X_i}$ is the mole fraction of each oxide.

The molar volume values ($(V_m)_{exp}$) were then calculated using equation (8),

$$(V_m)_{\exp} = \sum (M_i / \rho_{\exp}) \quad (8)$$

where $\mathbf{M_i}$ is the main molecular weight of a sample in (g/mol). The empirical molar volume values were also calculated using the same equation (no. 8), with replacing ($\boldsymbol{\rho_{exp}}$) by ($\boldsymbol{\rho_{emp}}$) values.

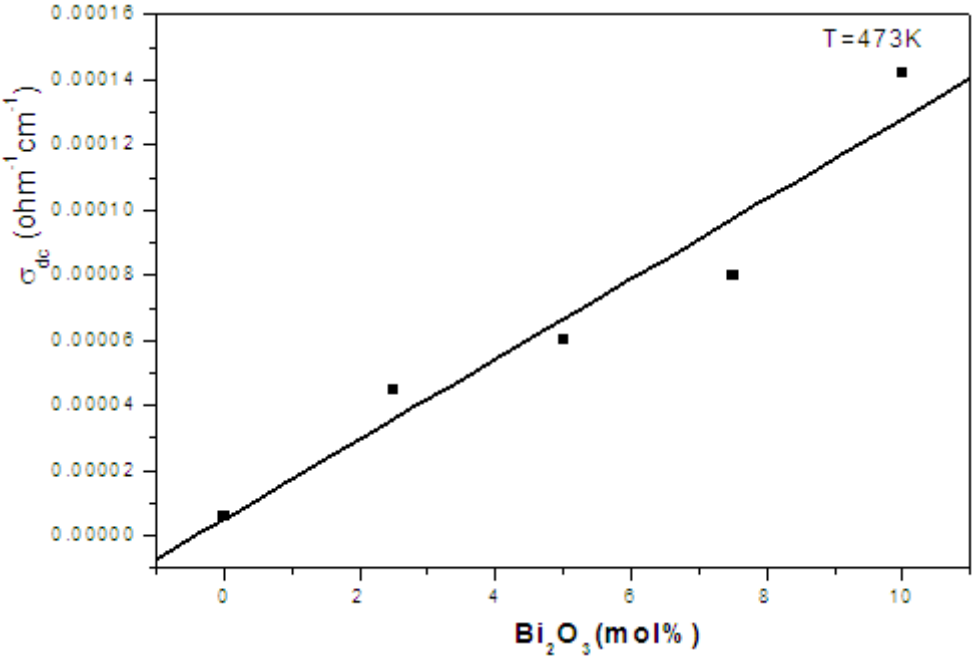

Figure (6). The dc conductivity as a function of Bi_2O_3 content at a fixed temperature (473 K)

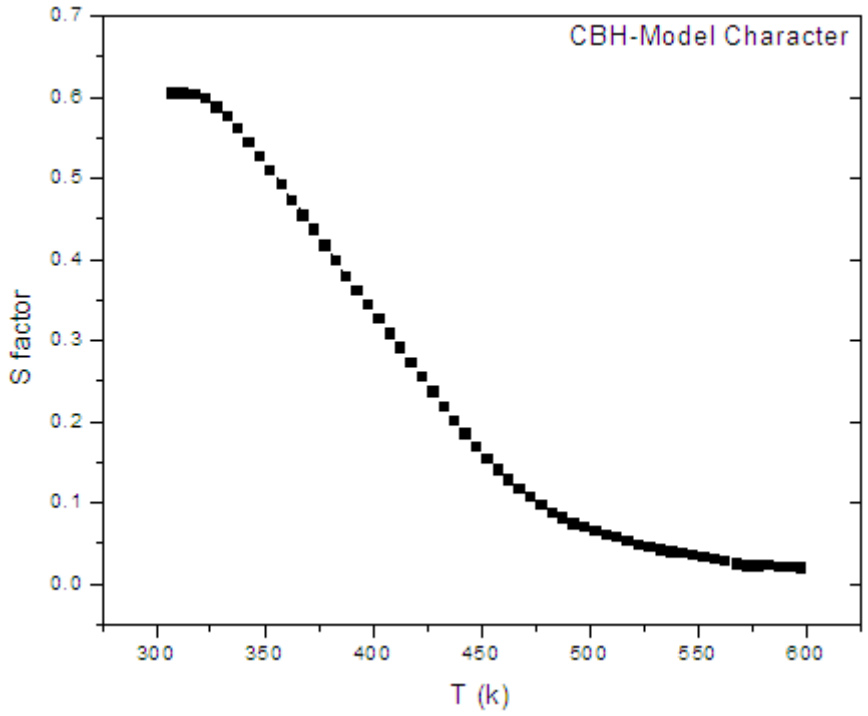

Figure (7). The variation of the s-factor with temperature for the sample containing 7.5 mol% Bi_2O_3, as representative curve

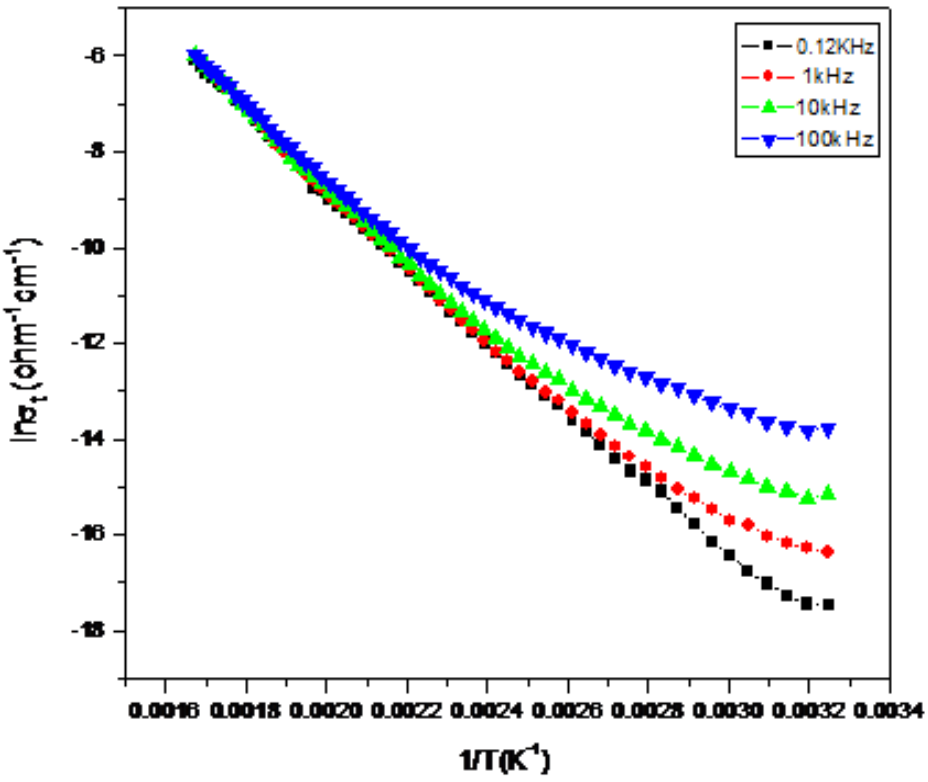

Figure (8). The variation of ln σ_t verses the reciprocal of temperature at four different frequencies for the sample containing 7.5 mol% Bi_2O_3, as representative curve

Figure (9), exhibits the variation of both the experimental and empirical density values as a function of Bi_2O_3 content for comparison, where both values show gradual linear increase. This may be due to the gradual introducing of the heavy Bi^{3+} cations replacing the lighter P^{5+} cations. It is observed also that the empirical density values are usually larger than those obtained experimentally. This can be taken as evidence for the pure glassy state of the present samples.

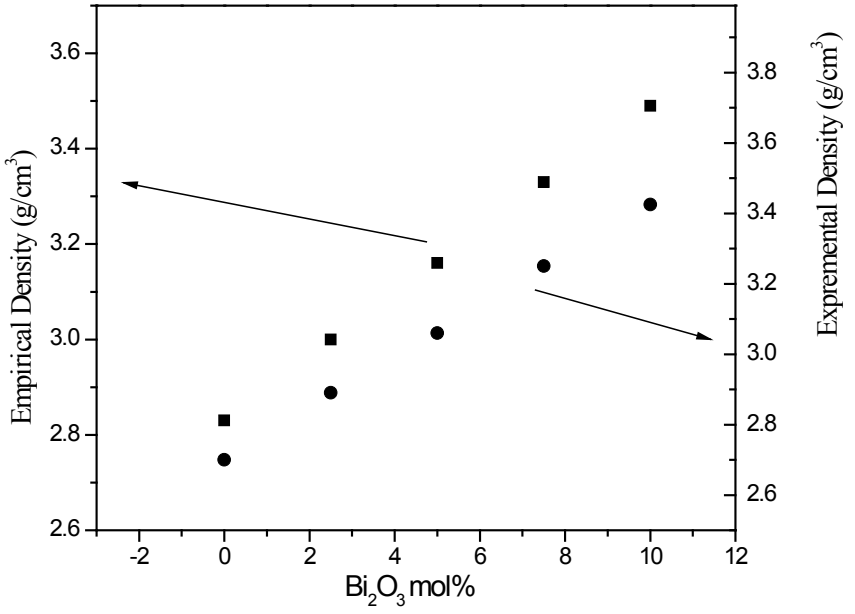

Figure (9). The variation of the experimental and empirical densities as a function of Bi_2O_3 content

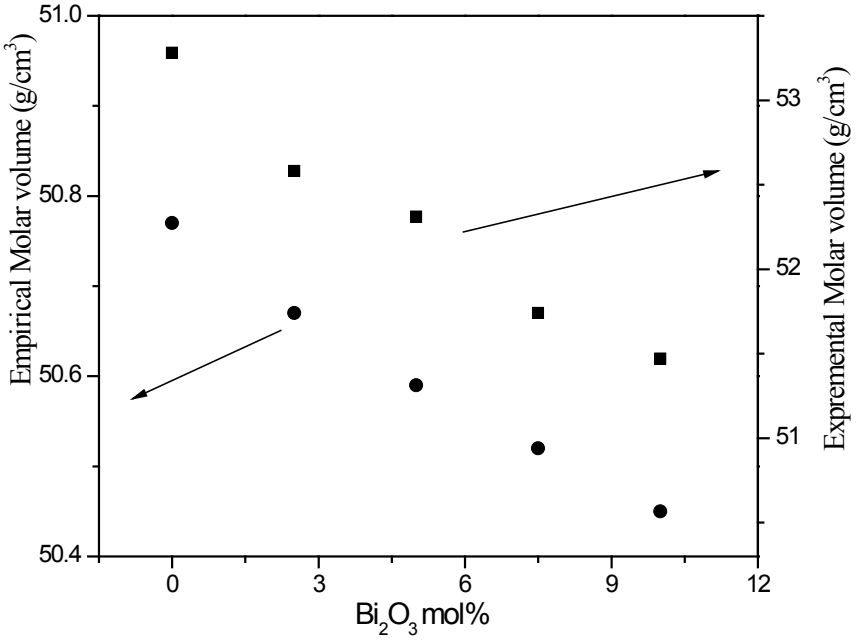

Figure (10). The variation of the experimental and empirical molar volume values as a function of Bi_2O_3 content

Table (2). The change of both the experimental and empirical density and molar volume values as a function of Bi_2O_3 content

Bi_2O_3 mol %	$\rho_{exp.}$ (g/cm^3)	$\rho_{emp.}$ (g/cm^3)	$V_{m\ exp.}$ (cm^3/mole)	$V_{m\ emp.}$ (cm^3/mole)
0	2.70	2.83	53.28	50.77
2.5	2.89	3.00	52.58	50.67
5	3.06	3.16	52.31	50.59
7.5	3.25	3.33	51.74	50.52
10	3.43	3.49	51.47	50.45

On the other hand, Figure (10) shows the change of both the experimental and empirical molar volume values as a function of Bi_2O_3 content, also for comparison, where both values show a gradual linear decrease and the empirical molar volume values appeared usually lower than those obtained experimentally. Such decrease in the molar volume values may be due to [29, 30]:

1- The formation of Fe–O bonds, at the expense of P–O bonds, which act to reticule the phosphate network structure.
2- The gradual decrease of the oxygen ion density in the glass network, since five oxygen atoms (in P_2O_5 molecule) are replaced by three only (in Bi_2O_3 molecule).

All the measured and the calculated values of both density and molar volume are exhibited in Table (2).

The higher values of the experimental molar volume in comparison to those obtained empirically confirm also the amorphous nature and the glassy state character of the studied samples, that observed previously by XRD analysis.

3.4. The Gamma-ray Attenuation Coefficients

The gamma-ray mass attenuation coefficients $(\mu/\rho)_m$ have been calculated using Win X-COM program (based on the mixture rule) at energies equal to 356 KeV (that of ^{135}Ba), 662 & 1173 KeV (those of ^{60}Co) and 1332 KeV (that of ^{137}Cs) as low energy γ-ray, using equation (9) [31],

$$\left(\frac{\mu}{\rho}\right)_{m(total)} = \sum_{i=0}^{n} w_i \left(\frac{\mu}{\rho}\right)_{mE} \quad (9)$$

where $(\mu/\rho)_{m(total)}$ is the total mass attenuation coefficient for a glass sample while $(\mu/\rho)_{mE}$ and w_i are the total mass attenuation coefficient and the fractional weight of each element in such glass sample.

Figure (11) represents the variation of $(\mu/\rho)_{m(total)}$ with the gradual increase of Bi_2O_3 at the expense of P_2O_5, where a gradual linear increase of $(\mu/\rho)_{m(total)}$ can be easily observed. It can be observed also that $(\mu/\rho)_{m(total)}$ increased with the gradual decrease of the gamma-ray photon energy, that is the highest $(\mu/\rho)_{m(total)}$ values are exhibited for the lowest gamma-ray photon energy (356 KeV, of ^{135} Ba).

On the other hand, The HVL values of the studied glass were also calculated according to equation (10), for the same gamma-ray energies.

$$HVL = 0.693 / \mu \quad (10)$$

Figure (12) exhibits the obtained values as a function of Bi_2O_3 content, where it can be seen obviously that the HVL decreased gradually with the gradual increase of Bi_2O_3 content. It decreased also with the gradual decrease of the gamma-ray photon energy, and the lowest values are exhibited for 356 Kev, (the gamma-ray energy emitted from ^{135}Ba).

The observed increase in the gamma-ray mass attenuation coefficient as well as the corresponding decrease in the half value layer of the studied glasses can be attributed to the gradual replacement of P_2O_5 by Bi_2O_3, since bismuth can be considered as a good attenuator cation for low energy γ-ray [19, 31-33].

However the best sample among all the studied glasses is that contains 10 mol% Bi_2O_3, which can be used as a good shielding material for low energy gamma-ray as well as for x-ray photon energy, due to:

i) Its high gamma-ray mass attenuation coefficient.
ii) Its low HVL.
iii) Its semiconducting properties which can release any formed charge on such shield.

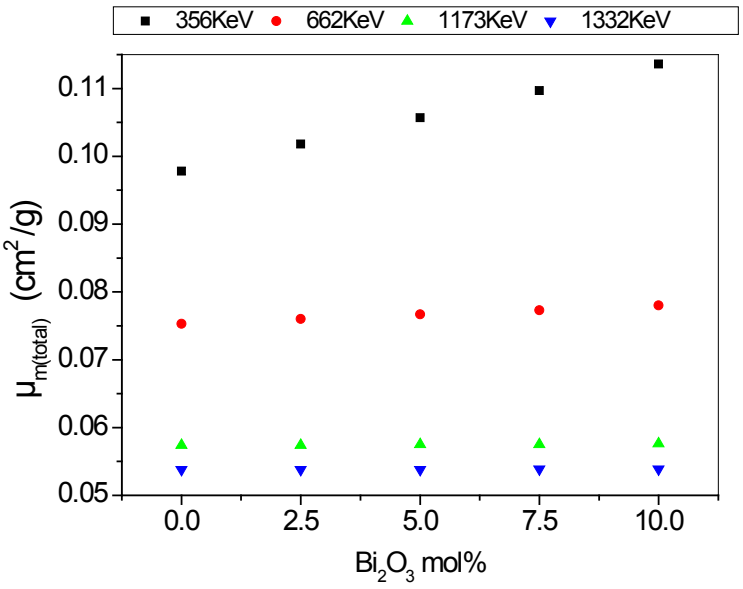

Figure (11). The mass attenuation coefficient of the studied glasses versus Bi_2O_3 content for different low gamma–ray energies

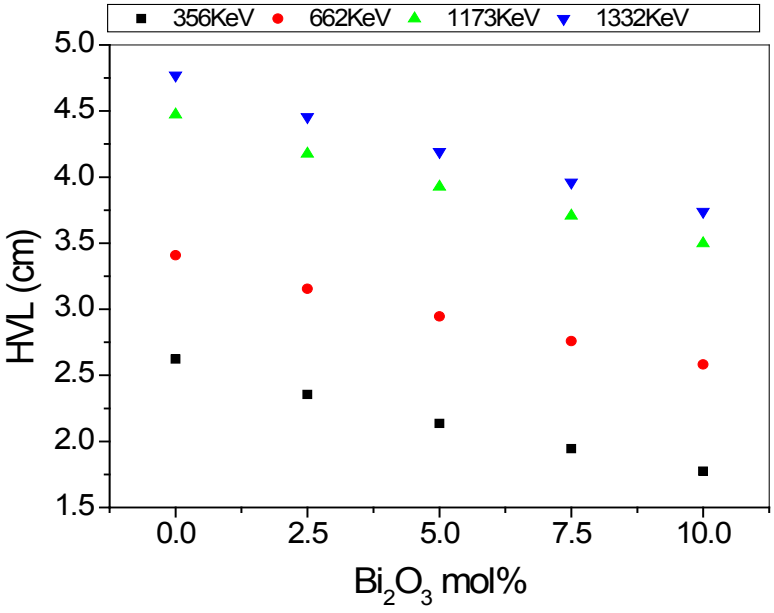

Figure (12). The HVL values of the studied glasses versus Bi_2O_3 content for different low gamma–ray energies

4. Conclusions

According to the obtained results and the supposed discussion, it can be concluded that all the investigated glasses appeared in good homogenous glassy phase. All Fe^{2+} ions occupy the tetrahedral coordination symmetry, but some Fe^{3+} occupy the tetrahedral coordination while the rest occupy the octahedral coordination state. In addition, the introduced Bi cations occupy the GNM positions and hence forced the Fe cations that occupy the octahedral coordination, acting as GNM to transfer to the tetrahedral symmetry to act as GNF.

The increase in the electrical conductivity depends strongly on the introduced Bi^{3+} cations, since they act to open the glass structure and to increase the amount of Fe^{2+} at the expense of Fe^{3+}, which in turn act to ease the mobility of Na^{+} cations and to increase the electron hopping in the glass networks. The CBH model is the predominant conduction mechanism. The change in the dielectric constant with the temperature does not show any peak, indicating that there is no change in the ferroelectric behavior of these glasses in the applied temperature range. The calculated electric modulus showed a relaxation peak shifted to the higher temperatures as the frequency was increased. Pseudo Cole-Cole diagram for all samples showed only one semicircle arc indicting a single relaxation process. Also the introduced Bi_2O_3 act to increase the density and to decrease the molar volume values.

It can be concluded also, from the study of $(\mu/\rho)_m$, that as Bi_2O_3 was gradually increased the gamma-ray mass attenuation coefficient increased while the HVL decreased, and the sample containing 10 mol% Bi_2O_3 can be used as good shielding material for low gamma-ray and x-ray photon energies.

REFERENCES

[1] R. H. Doremus, “Glass Science”, Wiley, London (1973).

[2] S. W. Martin, J. Amm. Ceram. Soc., 74 (1991) 1767.

[3] F. Borsa, D. R. Torgeson, S. W. Martin and H. K. Patel, Phys. Rev. (B), 46 (1992) 795.

[4] M. Zafar, A. Mausli and P. P. S. Prasad, “Handbook of solid state batteries and capacitors”, World Science, New York (1995).

[5] K. M. Ereiba, A. S. Abd Raboh and A. G. Mostafa, Nature and Science, 12 (5) (2014) 97.

[6] O. Deparis, F. P. Mezzapesa, C. Corbari, P. G. Kazansky and K. Sakaguchi, J. Non-Cryst. Solids, 351 (2005) 2166.

[7] W. H. Dumbaugh and J. C. Lapp, J. Amm. Ceram. Soc., 75 (1992) 2315.

[8] S. Hazra, S. Mandal and A. Ghosh, Phys. Rev. (B), 56 (1997) 8021.

[9] L. Baia, R. Stefan, W. Kiefer, J. Popp and S. Simon, J. Non-Cryst. Solids, 303 (2002) 379.

[10] L. Montagne, G. Palavit and G. Mairesse, Phys. Chem. Glasses, 37 (1996) 206.

[11] L. Montagne, G. Palavit and G. Mairesse, M. Draoui, K. Aomari and M. S. Idrissi, Phys. Chem. Glasses, 38 (1997) 15.

[12] A. Shaim and M. Et-Tabirou, Ann. Chem. Sci. Mater., 28 (2003) 17.

[13] Z. Ahaman, M. Et-Tabirou and M. Hafid, Phase Trans., 56 (1996) 247.

[14] A. Shaim, M. Et-Tabirou, L. Montagne and G. Palavit, Phys. Chem. Glasses, 44 (2003) 26.

[15] A. Chahine and M. Et-Tabirou, Mater. Res. Bull., 37 (2002) 1973.

[16] A. Chahine, M. Et-Tabirou and J. L. Pascal, Mater. Lett. 58 (2004) 2776.

[17] B. V. R. Chowdari, K. F. Mok, J. M. Xie and R. Gopalakrisnan, Solid State Ionics, 76 (1995)189.

[18] H. A. Saudi, A. G. Mostafa, N. Sheta, S. U. El Kameesy and H. A. Sallam, Physica (B), 406 (2011) 4001.

[19] A. G. Mostafa, H. A. Saudi, M. Y. Hassaan, S. M. Salem and S.S. Mohammad, American J. Modern Physics, 4 (4) (2015) 149.

[20] R. D. Husung, and M. Robert Doremus, J. Sci., 5 (1990) 10.

[21] A. G. Mostafa, G. Yahya, K.A. Ali, M. Gabr, N.S. Gomma, and N.A. Eissa, Solid State Commun., 131 (11) (2004) 729.

[22] M. Shapaan, E. R. Shabaan, and A. G. Mostafa, Phys. (B) Condens. Matter, 404 (14) (2009) 2058.

[23] F. Abdel-Wahab, A.G. Mostafa, A.E. Belal, and E.M. El-Agwany, Mater. Chem. Phys., 93 (1) (2005) 243.

[24] A. G. Mostafa, M. Y. Hassaan, A. B. Ramadan Z. A. Hussein and A. Y. Abdel-Haseib, Nature and Science, 11 (5) (2013) 148.

[25] A. M. Abdel-Ghany, A. A. Bendary, T. Z. Abou-El-Nasr, M. Y. Hassaan and A. G. Mostafa, Nature and Science, 12 (6) (2014) 139.

[26] P. Charles and Jr. Poole "Electron Spin Resonance" 2nd edd. John Wiley & Sons Inc. (1983).

[27] S. S. Fouad, A. E. Bekheet and A. M. Farid, J. Physica (B), 322 (2002) 163.

[28] M. Shapaan, S. A. El-Badry, A. G. Mostafa, M. Y. Hassaan, and M. H. Hazzaa, J. Phys. Chem. Solids, 73 (3) (2012) 407.

[29] A. G. Mostafa, Turk. J. Phys., 26 (2002) 441.

[30] A.G. Mostafa, M. A. Salem and Z. A. El-Hadi, J. Mater. Science & Technology, 18 (5) (2002) 391.

[31] D. F. Jackson and D. J. Hawkes, Phys. Rep., 70 (1981) 169.

[32] L. Gerward, N. Guilbert, K. B. Jensen and H. Levring, Radiat. Phys. Chem., 60 (2001) 23.

[33] H. comsan, A. M. Osman, A. M. Abd al- monem and A. R. Elsersy, J. Radiation Phy. Chem., 102 (2014) 167.